Supplementary File: Classification of Myocardial Blood Flow Based on Dynamic Contrast Enhanced Magnetic Resonance Imaging Using Hierarchical Bayesian Model

Yalei Yang
The University of Glasgow, Glasgow, UK.
E-mail: y.yang.2@research.gla.ac.uk
Hao Gao
The University of Glasgow, Glasgow, UK.
Colin Berry
The University of Glasgow, Glasgow, UK.
David Carrick
University Hospital Hairmyres, Glasgow, UK.
Aleksandra Radjenovic
The University of Glasgow, Glasgow, UK.
Dirk Husmeier
The University of Glasgow, Glasgow, UK.

A. The acquisition of input contrast concentration

We aquire the input contrast concentration $C_{in}(t_j)$ from the blood pool signal. Firstly, we manually observe the blood pool in the images. Then, we use a 3×3 square to record the same blood pool area in all images. Finally, we use the average value of signal intensities in the square to be the blood pool signal and use the signal to concentration equation (equation (1) in the main paper)to transfer the signal values to the concentration values.

B. An alternative selection of prior distributions

In the main text, log-Gaussian priors are used for the logarithm of parameters $\mathbf{\Theta}_i$. There is an alternative selection. We can use Gamma distributions as their prior distributions. To be specific, for the term $P(\mathbf{\Theta}_i|\mathbf{\Theta}_{-i}, \mathbf{\Gamma}, k^i, k^{-i})$, we have:

$$\begin{aligned} P(\mathbf{\Theta}_i|\mathbf{\Theta}_{-i}, \mathbf{\Gamma}, k^i, k^{-i}) \propto & \Gamma(A_i|\alpha_{A,k^i}, \beta_{A,k^i})\Gamma(\omega_i|\alpha_{\omega,k^i}, \beta_{\omega,k^i}) \\ & \Gamma(\lambda_i|\alpha_{\lambda,k^i}, \beta_{\lambda,k^i})P(\mathbf{\Theta}_i|\mathbf{\Theta}_{-i}, k^i, k^{-i}). \end{aligned} \tag{1}$$

Now, we derive the conditional posterior distributions for the hyperparameters $\mathbf{\Gamma} = \{\alpha_{A,k^i}, \beta_{A,k^i}, \alpha_{\omega,k^i}, \beta_{\omega,k^i}, \alpha_{\lambda,k^i}, \beta_{\lambda,k^i}\}$. $P(\mathbf{\Gamma}|\alpha^{**}, \beta^{**})$ is the prior distribution for hyperparameters $\mathbf{\Gamma}$ where we let $(\alpha^{**} = 0.01, \beta^{**} = 0.01)$. In this way, $P(\alpha_{A,k^i}, \beta_{A,k^i}|\alpha^{**}, \beta^{**})$ is:

$$P(\alpha_{A,k^i}, \beta_{A,k^i}|\alpha^{**}, \beta^{**}) = \Gamma(\alpha_{A,k^i}|\alpha^{**}, \beta^{**})\Gamma(\beta_{A,k^i}|\alpha^{**}, \beta^{**}). \tag{2}$$

The prior distributions for other hyperparameters can be set similarly. $P(\mathbf{\Gamma}|\alpha^{**},\beta^{**})$ is the product of all of them because all these hyperparameters are independent. The conditional distribution of $\alpha_{A,k^i}, \beta_{A,k^i}$ is given by

$$\begin{aligned} & P(\alpha_{A,k^i=\psi}, \beta_{A,k^i=\psi}|\{A_i, A_{-i}\}_{i|k^i=\psi}, k^i=\psi, \alpha^{**}, \beta^{**}) \\ = \; & P\Big(\alpha_{A,k^i=\psi}, \beta_{A,k^i=\psi}|\alpha^{**}, \beta^{**}\Big) \prod_{i|k^i=\psi} \Gamma\Big(A_i|\alpha_{A,k^i=\psi}, \beta_{A,k^i=\psi}\Big) \end{aligned} \tag{3}$$

where $\psi \in \{0,1\}$ is the binary lesion indicator, and $P(\alpha_{A,k^i=\psi}, \beta_{A,k^i=\psi}|\alpha^{**},\beta^{**})$ can be found in equation (2). The conditional posterior distributions for $\{\alpha_{\omega,k^i=\psi}, \beta_{\omega,k^i=\psi}, \alpha_{\lambda,k^i=\psi}, \beta_{\lambda,k^i=\psi}\}$ can be derived similarly. For $\beta_{A,k^i=\psi}$, its conditional posterior distribution is:

$$\begin{aligned} & P(\beta_{A,k^i=\psi}|\{A_i\}_{i|k^i=\psi}, \alpha_{A,k^i=\psi}, \alpha^{**}, \beta^{**}, k^i=\psi) \\ = \; & \Gamma\Big(\alpha^{**} + \sum_{i|k^i=\psi} \alpha_{A,k^i=\psi}, \beta^{**} + \sum_{i|k^i=\psi} A_i\Big). \end{aligned} \tag{4}$$

For $\alpha_{A,k^i=\psi}$, the samples from its conjugate prior cannot be sampled directly. In this way, a Gamma prior is used for it and Metropolis-Hastings algorithm will be used in the sampling scheme.

Figures (1) and (2) show the comparisons using the Gamma prior and Gaussian prior given $T_{k^i} = 0.1$ and $T_{\text{Fermi}} = 1$. The difference in the results obtained with a log-Gaussian versus a Gamma prior was found to be minor, which suggests that the choice of functional family for the prior distributions on the Fermi parameters $\mathbf{\Theta}_i$ is not critical, as long as the distributions are consistent with the positivity constraint of the Fermi parameters, i.e. have positive support.

C. Supplementary Data

In this section, some extra supplementary data and results are shown to strengthen our conclusions.

C.1. Results

In this section, we show the comparisons of our methods and alternative models based on 3 sets of DCE-MRI myocardial perfusion data. According to the model selection result in the main paper, the values of hyperparameters are chosen to be $T_{k^i} = 0.1$ and $T_{\text{Fermi}} = 1$. Figure (3), (4) and (5) show the comparisons of the MBF estimations between the Fermi model and the HBM method proposed in this work. The performances of the comparisons are consistent with the main paper.

Figure (6), (7) and (8) show the comparisons of the classifications bewtween the GMM based on Fermi and the HBM method proposed in this work. The performances of the comparisons are consistent with the main paper.

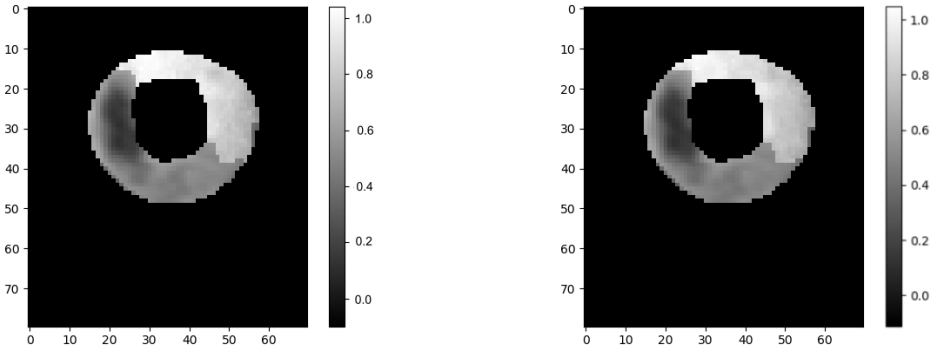

(a) log-Gaussian prior (b) Gamma prior

Fig. 1. MBF Comparisons between different priors
These figures show the estimations of the MBF (rescaled within [0,1]) between different prior distributions for Fermi parameters. The greyscale denotes the value of MBF. The pixels inside and outside of the ring (myocardium) are background. Panel (a) shows the estimations using log-Gaussian priors based HBM. Panel (b) shows the estimations using Gamma priors based HBM.

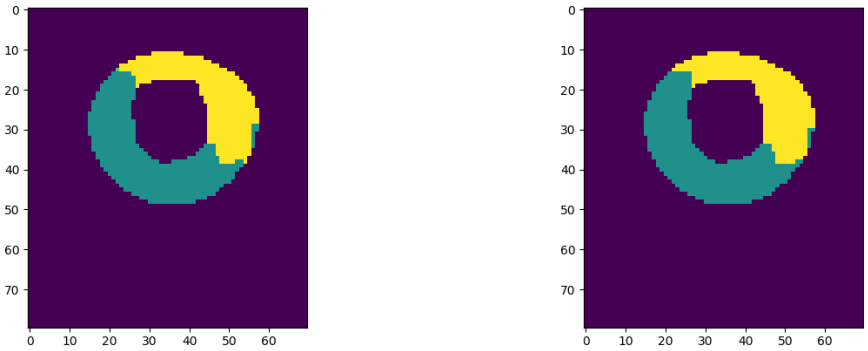

(a) log-Gaussian prior (b) Gamma prior

Fig. 2. Classification Comparisons between different priors
The figure shows the pixel-wise myocardial tissue classification between different prior distributions for Fermi parameters. The yellow region indicates healthy tissues and dark green region indicates lesions. The blue colour marks the background of the myocardial ring. The class assignments are based on the estimated posterior class probabilities, as explained in the main text. Panel (a) shows the classification using log-Gaussian priors based HBM. Panel (b) shows the classification using Gamma priors based HBM.

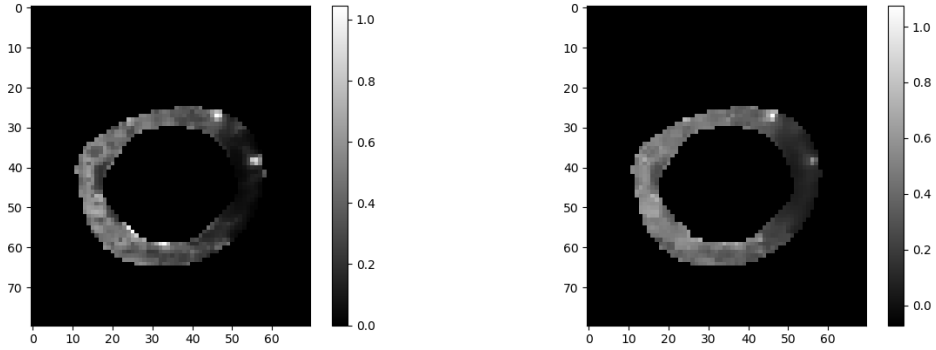

(a) Fermi model (b) proposed HBM

Fig. 3. MBF estimations for serial 25
These figures show the estimations of the MBF (rescaled within [0,1]). The greyscale denotes the value of MBF. The pixels inside and outside of the ring (myocardium) are background. Panel (a) shows the Fermi model fitted by least-squares. Panel (b) shows the MBF estimations using the HBM illustrated in this paper.

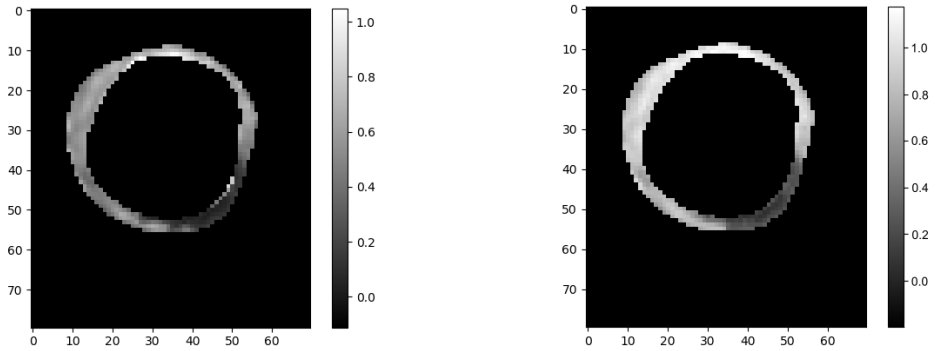

(a) Fermi model (b) proposed HBM

Fig. 4. MBF estimations for serial 26
These figures show the estimations of the MBF (rescaled within [0,1]). The greyscale denotes the value of MBF. The pixels inside and outside of the ring (myocardium) are background. Panel (a) shows the Fermi model fitted by least-squares. Panel (b) shows the MBF estimations using the HBM illustrated in this paper.

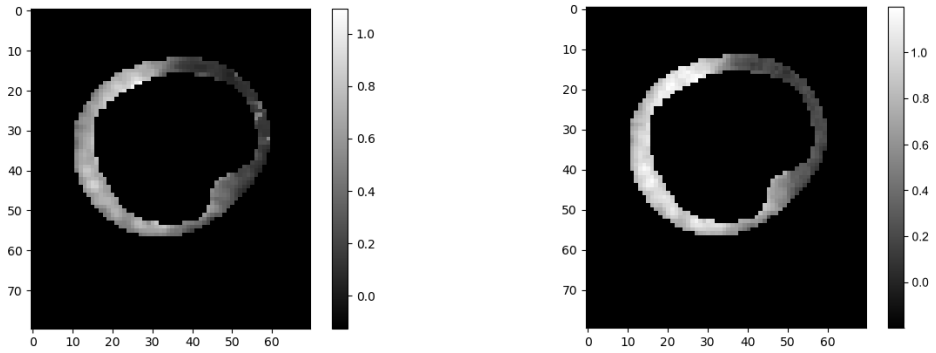

(a) Fermi model (b) proposed HBM

Fig. 5. MBF estimations for serial 27
These figures show the estimations of the MBF (rescaled within [0,1]). The greyscale denotes the value of MBF. The pixels inside and outside of the ring (myocardium) are background. Panel (a) shows the Fermi model fitted by least-squares. Panel (b) shows the MBF estimations using the HBM illustrated in this paper.

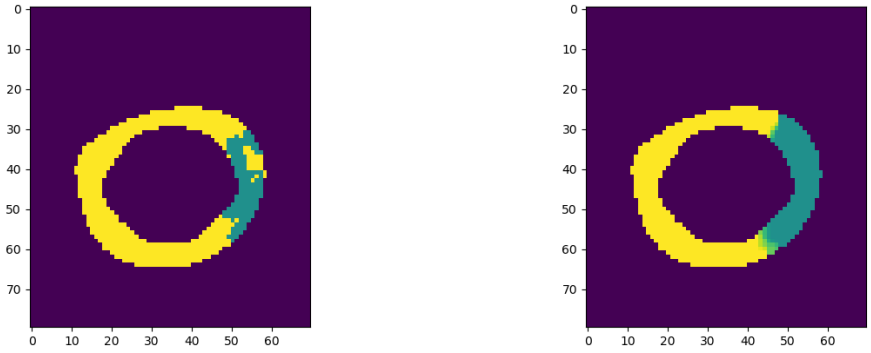

(a) GMM based on Fermi model (b) proposed HBM

Fig. 6. The classifications for serial 25
The figure shows the pixel-wise myocardial tissue classification into the three classes *lesion* (dark green), *healthy* (yellow) and *uncertain* (light green). The blue colour marks the background of the myocardial ring. The class assignments are based on the estimated posterior class probabilities, as explained in the main text. Panel (a) shows the classification based on Fermi estimated MBF using Gaussian Mixture Model. Panel (b) shows the classification result based on the HBM illustrated in this work.

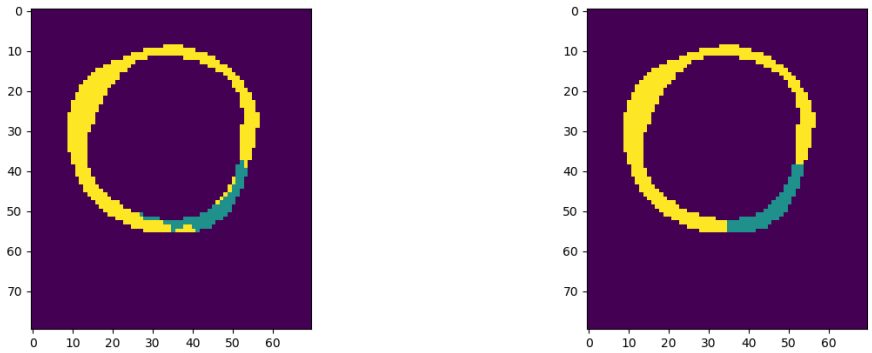

(a) GMM based on Fermi model (b) proposed HBM

Fig. 7. The classifications for serial 26
The figure shows the pixel-wise myocardial tissue classification into the three classes *lesion* (dark green), *healthy* (yellow) and *uncertain* (light green). The blue colour marks the background of the myocardial ring. The class assignments are based on the estimated posterior class probabilities, as explained in the main text. Panel (a) shows the classification based on Fermi estimated MBF using Gaussian Mixture Model. Panel (b) shows the classification result based on the HBM illustrated in this work.

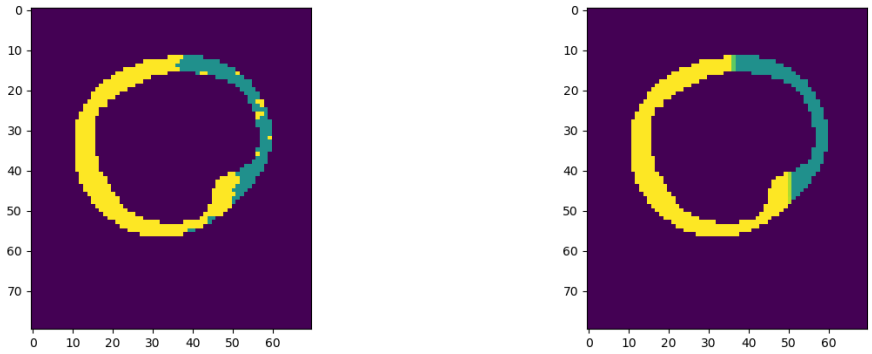

(a) GMM based on Fermi model (b) proposed HBM

Fig. 8. The classifications for serial 27
The figure shows the pixel-wise myocardial tissue classification into the three classes *lesion* (dark green), *healthy* (yellow) and *uncertain* (light green). The blue colour marks the background of the myocardial ring. The class assignments are based on the estimated posterior class probabilities, as explained in the main text. Panel (a) shows the classification based on Fermi estimated MBF using Gaussian Mixture Model. Panel (b) shows the classification result based on the HBM illustrated in this work.